Surface Pressure Measurement on a Rotating Blade of Field Horizontal Axis Wind Turbine in Yawed Condition*

Takao MAEDA** and Hideyuki KAWABUCHI**

This paper shows the pressure distribution at the 50% radial section of a rotor blade of 10 m-diameter wind turbine in yawed operation. The pressure sensors were mounted on the blade, and local inflow angle and local dynamic pressure were measured with the use of five hole Pitot tubes at 1 chord length upwind of the blade leading edge. It was found that the normal force coefficient in yawed condition decreases compared to that for non-yawed condition. Even if local angle of attack and the relative inflow velocity are the same, pressure distribution shows differences due to the local slip angle. The tufts flow-visualization on the rotating blade was carried out by setting a video camera on the rotating system. Separation in the region of middle chord to trailing edge on suction surface is thought to be the main reason of the reduction of normal force coefficients.

Key Words: Fluid Machinery, Wind Mill, Blade, Pressure Distribution, Stall, Unsteady Flow, Yaw Effects

1. Introduction

Since energy density of the wind is small, improvement in performance of wind turbine blade is indispensable for taking out energy from the wind efficiently. Generally, wind turbine blade airfoil is designed by 2D numerical analysis, and verified in the wind tunnel test. However, in the field, the flow around the wind turbine blade is unsteady, and it becomes more complex due to the effects of Coriolis force, centrifugal force and three-dimensional flow. Therefore, it becomes important to investigate the unsteady aerodynamic force acting on the rotor blade. Unsteady Aerodynamic Experiment and the NREL Full-Scale Wind Tunnel Experiment are without doubt the major contributions to the community working on wind turbine aerodynamics[1]-[3]. It is uncertain that sufficiently detailed field measurements exist for validating aerodynamic models against the actual three-dimensional, unsteady flow. Complexity of the flow behavior on the wind turbine blade makes it necessary to provide more data for a broad range of experimental conditions.

In this study, with focus on blade characteristic affecting the wind turbine performance, field experiements were performed on a 10 m-diameter wind turbine. Surface pressure measurements were carried out. Characteristics of the aerodynamic forces acting on rotor blade are clarified. In the previous studies, the present authors had clarified aerodynamic force at 70% radial section, where the flow is considered to be close to two-dimensional flow[4]. The following data compare the performance characteristics of the rotor through analyzing the three-dimensional features of the flow at 50% radial section on the rotor blade. The change of section characteristics due to a nacelle yaw angle was clarified. Moreover, the flow behavior on the rotating blade was observed through tufts flow-visualization method by setting a video camera on the rotating system.

* Received 21st July, 2004 (No. 04-4166)

** Department of Mechanical Engineering, Mie University, 1515 Kamihama-cho, Tsu, Mie 514–8507, Japan.
E-mail: maeda@mach.mie-u.ac.jp

2. Nomenclature

c : chord length [m]
C_m : moment coefficient at 0.25 chord station, Eq. (4)
C_n : normal force coefficient, Eq. (2)
C_p : pressure coefficient, Eq. (1)
C_t : tangential force coefficient, Eq. (3)
p : pressure at blade surface which offset centrifugal force [Pa]
p_d : dynamic pressure at $1c$ upwind of blade leading edge [Pa]
R : rotor diameter [m]
r : position of radial direction [m]
Re : Reynolds number = Wc/ν
U : wind speed [m/s]
W : inflow velocity at $1c$ upwind of blade leading edge [m/s]

x : distance from leading edge along airfoil chord [m]
y : distance perpendicular to airfoil chord [m]
α : local angle of attack at $1c$ upwind of blade leading edge [deg]
β : local slip angle at $1c$ upwind of blade leading edge [deg]
γ : blade twist angle [deg]
θ : blade pitch angle [deg]
σ : standard deviation of measured quantity per rotor revolution
ν : kinetic viscosity [m^2/s]
Φ : yaw angle [deg]
Ψ : azimuth angle [deg]

Subscript

C_n : normal force coefficient
i : i-th pressure tap number
α : local angle of attack
β : local slip angle

3. Experimental Setup

3.1 Open air rotor research facility

Figure 1 shows a general view of the test wind turbine. This test wind turbine is a three-bladed upwind HAWT type which has variable pitch mechanism, a rated output of 8 kilowatts, a rotor diameter of 10 meters. A cylindrical tiltable tower supported the turbine at hub height of 13.3 meters. The rotor revolution, constant speed of 80 rpm, was amplified 9 times through an intermediate shaft by speed up gear mechanism using timing belts and transmissions. A yaw drive motor was attached between the nacelle and the tower and it was adjustable to the wind direction. The yaw angle, which is positive in the counter-clockwise direction, was measured with a rotary encoder attached to the rotational shaft of the nacelle. The pitch angle of blade was measured by a potentiometer built in a power cylinder for the pitch drive. The power generation system is composed of an induction generator with a phase-advanced condenser. The wind speed was measured by a sonic wind speed meter set up at the same height as the hub of test turbine and 10 meters upstream of the wind turbine.

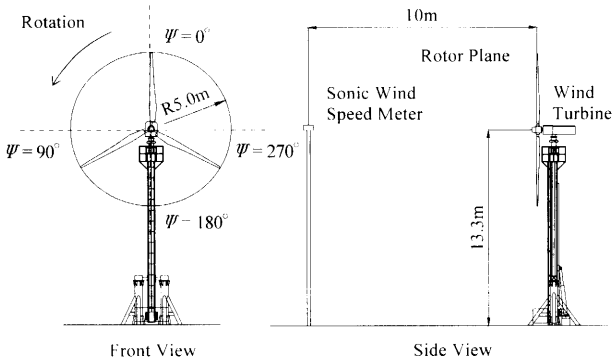

Fig. 1 Location of test wind turbine and wind speed meter

3.2 Test blade

Blade planform, taper and twist distributions are shown in Fig. 2. The blades used in this experiment were twisted and tapered. The spanwise airfoil distributions were formed with the airfoil of DU and NACA from the blade root to the tip. One of the blade was equipped with pressure taps at four radial sections of 32.5%, 50%, 70% and 90%. Each section has 60 pressure taps on the suction and pressure sides. Figure 3 shows the location of pressure taps on the rotor blade at the 50% radial section. The taps were more densely distributed near the blade leading edge to better investigate the pressure gradients present there.

Inflow angles were measured near the pressure taps using two five-hole probes. Probes were mounted at loca-

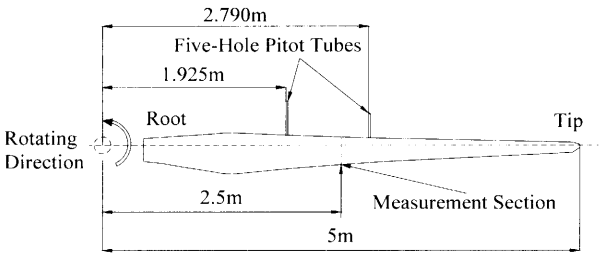

(a) Blade planform

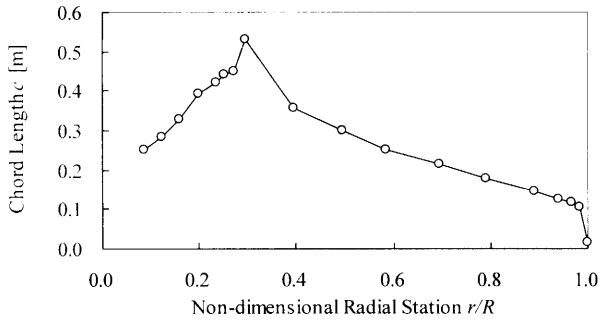

(b) Chord distribution

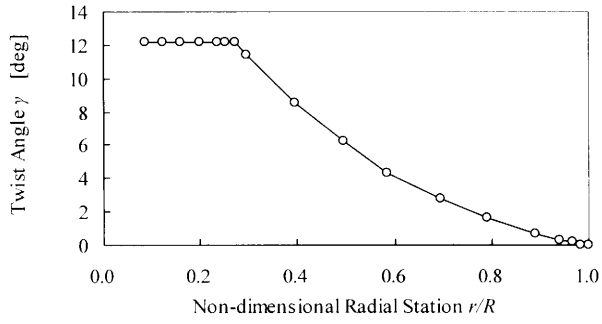

(c) Twist distribution

Fig. 2 Test blade

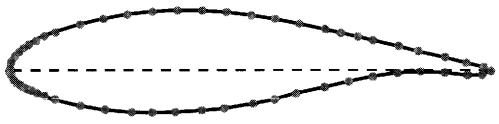

Fig. 3 Position of pressure taps on measurement section

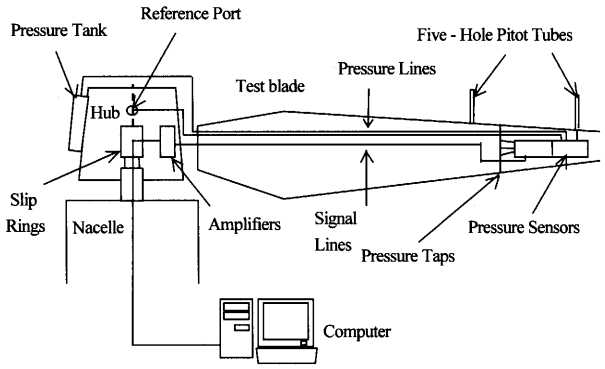

Fig. 4 Measurement system

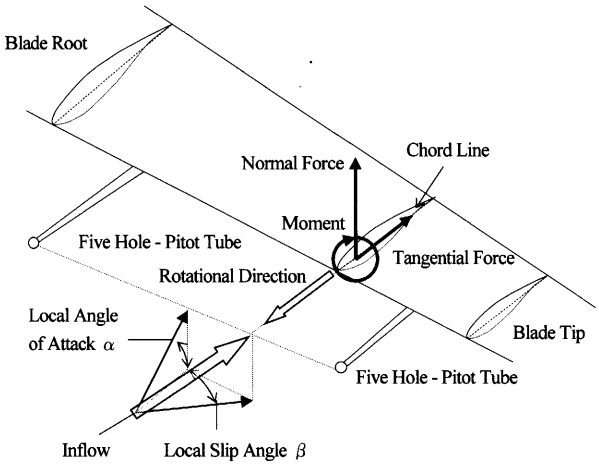

Fig. 5 Definition of normal force, tangential force, moment, local angle of attack and local slip angle

tions 0.385R and 0.558R, respectively, with the probe tip 1c upstream of the blade leading edge. Five-hole probe pressures were measured and the inflow angles were derived from these measurements.

3.3 Measurement system

Figure 4 shows pressure measurement system. The instantaneous pressures were simultaneously measured with the use of multi-ports pressure transducers in the rotating blade. A total of 64 ports were imbedded inside the blade. Scanivalve ZOC23B transducers were used for the pressure measurements. The signals from the sensors were amplified up to 100 times in the rotational system and were transmitted through the platinum slip rings to the stationary system. Sampling frequency of 90 Hz corresponded to the timer on the A/D board. Referring to the rotor revolution of 80 rpm, the sampling interval corresponded to an increment azimuth angle of 5.3 degrees. One data set for field test was composed with 7 400 data in 90 seconds. The pressure data were separately collected at each radial section by limiting of number of sensor ports and A/D converters. Collected data at each radial section include the data measured at yaw angle of 0, ±30 and ±45 degrees. Azimuth angle was measured using a rotary encoder, which was measured counterclockwise. The angle was defined as 0 degree (see Fig. 1), when blade tip was at the uppermost vertical position (12 o'clock azimuthal position).

3.4 Definitions and non-dimensionalization

Due to the unsteadiness of wind speed and the nonuniformity of the inflow velocity distribution to the blade span direction due to the induced velocity, it was difficult to determine the angle of attack at measured section. By using two five-hole probes, installed next to the measured radial section, whose length was as long as chord length of each installed section, the inflow angle and dynamic pressure at the tip of every five-hole pitot probe were measured. Through linear interpolation, the local angle of attack α, local slip angle β and dynamic pressure of the inflow velocity p_d, were defined at the measured radial section.

The pressure on the rotor blade surface depends on the inflow velocity, local angle of attack and blade surface shape. Therefore, the data were reduced by defining the pressure coefficient C_p as a non-dimensional parameter. In this study, pressure p_i at the i-th pressure tap on the measurement section was non-dimensionalized by the dynamic pressure of the inflow velocity p_d, and the pressure coefficient C_{p_i} was calculated from the following equation.

$$C_{p_i} = p_i / p_d \tag{1}$$

Note that the centrifugal effects were excluded from the pressure data.

Definition of the aerodynamic properties based on the condition of the uniform flow is not applicable in case of unsteady wind and non-uniform flow, such as field experiments. To simplify the analysis, in this paper the definition of the local aerodynamic properties is based on Cartesian coordinate system fixed to the blade. Figure 5 shows the schematic view of the definition of local angle of attack, normal force, tangential force, moment and local slip angle. The local angle of attack was determined by interpolation of local angle of attack obtained from two five-hole probes. The local slip angle, β, is defined as the angle between the local inflow direction and the five-hole probe direction and is measured in the blade planform plane. The force parallel to the chord direction was described as tangential force and perpendicular to the chord direction was described as normal force. The moment was calculated based on $x/c = 0.25$. Normal force coefficients, C_n, tangential force coefficients, C_t, and moment coefficient, C_m, are non-dimensionalized and normalized according to the following formulas:

$$C_n = \sum_{i=1}^{n} \frac{p_i}{p_d} \frac{\Delta x_i}{c} = \frac{1}{c} \sum_{i=1}^{n} C_{p_i} \Delta x_i \tag{2}$$

$$C_t = \sum_{i=1}^{n} \frac{p_i}{p_d} \frac{\Delta y_i}{c} = \frac{1}{c} \sum_{i=1}^{n} C_{p_i} \Delta y_i \tag{3}$$

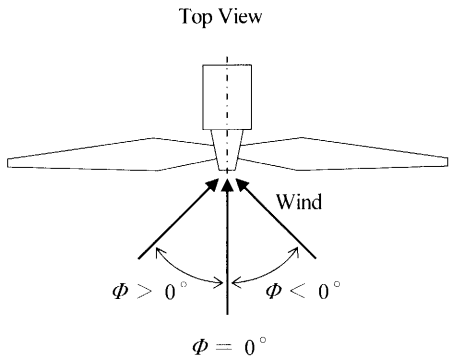

Fig. 6 Definition of yaw angle Φ

$$C_m = \frac{1}{c^2}\sum_{i=1}^{n}\left(C_{p_i} l_{t_i} \Delta x_i + C_{p_i} l_{n_i} \Delta y_i\right) \tag{4}$$

where, Δx_i, Δy_i, l_{n_i} and l_{t_i} are small lengths along the chord direction at the i-th pressure tap, small lengths to a direction perpendicular to the chord line at the i-th pressure tap, the moment arm lengths to the direction perpendicular to the chord line and parallel to the chord line, respectively. Positive normal force C_n was thought to be oriented from the pressure surface toward the suction surface. Tangential force, C_t, was defined as positive when directed from the leading edge toward the trailing edge. C_m was defined a clockwise rotation as positive, based on $x/c = 0.25$. Moreover, local slip angle β was defined as a radial direction inflow angle in the blade upstream, on the basis of five-hole probe. It was considered positive when the inflow velocity showed radial outward direction.

3.5 Yaw angle

In this paper, the yaw angle was defined as the angle between the nacelle direction and the wind speed, as shown in Fig. 6. The data were collected for the yaw angle in the interval [−45, +45] degrees with a step of 15 degrees. The yaw angle was controlled automatically and it followed the wind direction change. Due to the time lag between the wind direction change and nacelle direction change, a tested yaw angle was determined when it was within ±7.5 degrees of the required value. For example the data pretended to be taken for the yaw angle 30 degrees, were all the data obtained for a yaw angle between 22.5 degrees and 37.5 degrees.

3.6 Tufts flow-visualization

In addition to surface pressure measurements, flow visualization through surface tuft method of the instrumented blade was performed. Tufts, made of woolen yarn of 2.5 mm in diameter, and of 15% of the blade chord length of the corresponding to be attached section in length, were set on the suction surface. The tufts were set every 5% of the airfoil chord length to the blade chord direction, and every 100 mm to the blade span direction. In order not to interfere with pressure data, collected simultaneously with flow visualization, the tufts were not set on the area around the measured section, 100 mm from measured section to the blade root side and 100 mm from measured section to the blade tip side. A CCD wireless digital color camera, fixed on a stand attached in the flange of the instrumented blade, was used for photography. The images data were transmitted from an antenna attached on the boss to a receiver on the ground, and data were taken by the personal computer through a signal cable. The sampling frequency, 30 Hz, was equivalent to the pressure data collection for every 16 degrees of azimuth angles.

Table 1 Experimental condition

	Measurement Condition
Wind Speed U [m/s]	3.9～10.4
Inflow Velocity W at 1c Upwind of Blade Leading Edge [m/s]	18.9～26.8
Reynolds Number Re	3.5×10^5～5.5×10^5
Pitch Angle θ [deg]	2.5～7.5

4. Experimental Results and Discussions

4.1 Data reduction

Field test data analyzed in this paper were measured with a sampling frequency of about 90 Hz with a total of 463 124 data collected. Table 1 lists the experimental conditions in this study. The wind condition and the rotor speed differs for every data. For the data reduction, average values and standard deviations were calculated for every rotor rotation, and, then, the BIN average was calculated for the local angle of attack at every 1 degree. Here, the BIN means the range of the value for carrying out the group division of the instantaneous value data. For example, the BIN average at every 1 degree in this study means that the data corresponding to α is the average value of data contained in the range of the width $(\alpha - 0.5, \alpha + 0.5)$ degree.

4.2 Change of the measured quantities against local angle of attack due to yaw angle

Figure 7 shows the section characteristics at the 50% spanwise station, with data reduction performed for yaw angle Φ of −45, 0, and 45 degrees, respectively. Figure 7 (a) shows normal force coefficient C_n against local angle of attack α. Note that compared to the data obtained for the yaw angle $\Phi = 0$ degree, C_n values at $\Phi = 45$ degrees tend to become slightly smaller for whole range of local angle of attack α. The same tendency is noticed for C_n values at yaw angle $\Phi = -45$ degrees, but the reduction rate is larger than the case where yaw angle is $\Phi = 45$ degrees. Figure 7 (b) shows tangential force coefficient C_t against local angle of attack α. There is no clear difference when comparing the data for yaw angles Φ of −45, 0, and 45 degrees. Figure 7 (c) shows moment coefficient C_m against local angle of attack α. Compared the data for different yaw angles, it is found that while C_m values

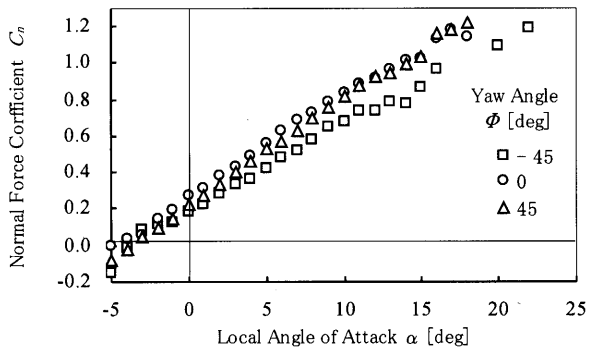

(a) Normal force coefficient C_n against local angle of attack α

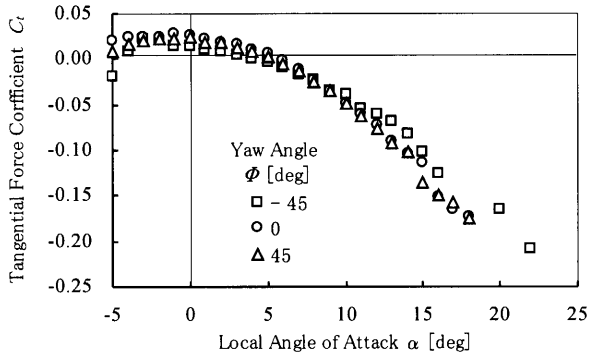

(b) Tangential force coefficient C_t against local angle of attack α

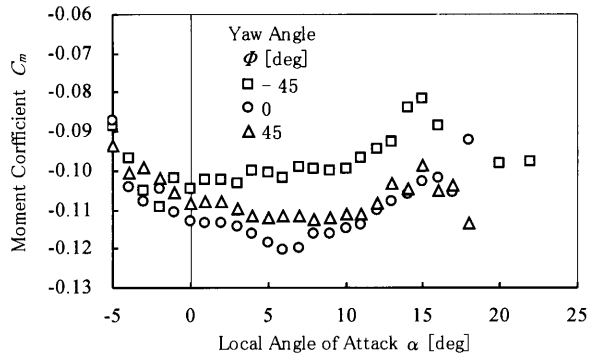

(c) Moment coefficient C_m against local angle of attack α

Fig. 7 Section characteristics in several yawed conditions

at $\Phi = 45$ degrees become larger than C_m values at yaw angle $\Phi = 0$ degree in the range of local angle of attack $-5 \leq \alpha \leq 10$ degrees, for yaw angle $\Phi = -45$ degrees C_m values become larger in whole range of local angle of attack α.

Figure 8 shows normal force coefficient C_n against yaw angle Φ, for three representative local angle of attack $\alpha = 5$, 10 and 15 degrees, respectively. Observing the graphs, it is noted that the C_n reaches a maximum at yaw angle between 0 and 15 degrees, and it has a decreasing tendency for yaw angles larger than 15 degrees and smaller than 0 degrees. However, although the tendency for C_n to become small when the yaw angle Φ becomes large above $\Phi = 15$ degrees, the reduction rate becomes smaller than those for $\Phi < 0$. Thus, in this case, it can be

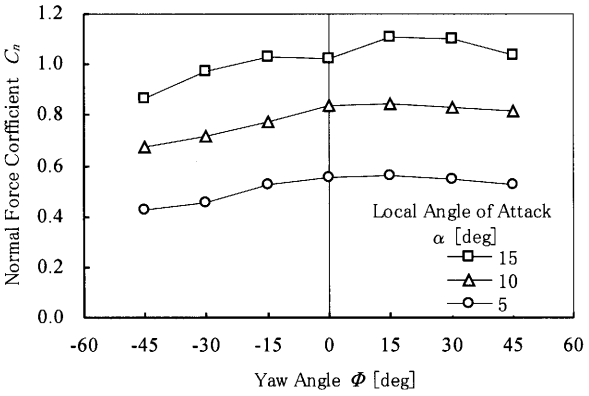

Fig. 8 Normal force coefficient C_n against yaw angle Φ

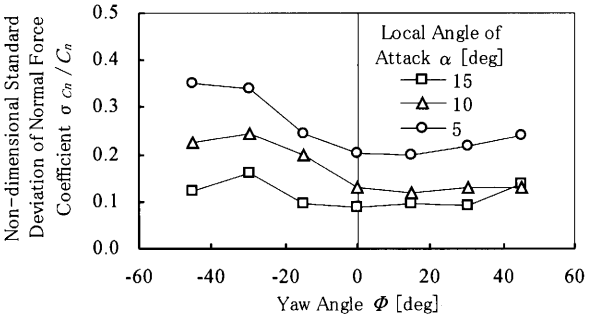

(a) Normal force coefficient C_n

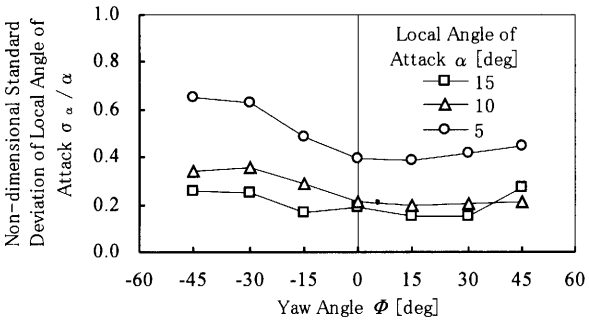

(b) Local angle of attack α

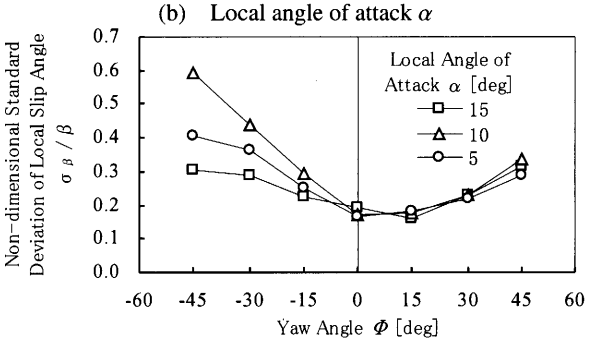

(c) Local slip angle β

Fig. 9 Non-dimensional standard deviation against yaw angle Φ

seen that the change of C_n value becomes asymmetrical about $\Phi = 0$ degrees. The reason and explanations for this phenomenon are given in the section 4.3.

Figure 9 shows non-dimensional standard deviation of the section characteristics during 1 rotor rotation. The

BIN averages were calculated for every local angle of attack α, but in the figure the data for three representative local angle of attack is shown. Figure 9(a) shows the non-dimensional standard deviation of normal force coefficient σ_{C_n}/C_n against yaw angle Φ, Fig. 9(b) shows non-dimensional standard deviation of local angle of attack σ_α/α against yaw angle Φ, and Fig. 9(c) shows non-dimensional standard deviation of local slip angle σ_β/β against yaw angle Φ, respectively. Notice the same trends against the yaw angle for all aerodynamic characteristics considered. The values of σ_{C_n}/C_n, σ_α/α, and σ_β/β increase for negative yaw angles and for yaw angles larger than 0 degrees. However, the rate of change is different in both sides of ordinate axis. It is proved that, when the value of yaw angle is negative, the change of aerodynamic forces acting on the rotor during one rotation become larger.

4.3 Change of the measured quantities against azimuth angle due to yaw angle

In the previous section, the variation of the section characteristics due to the change of yaw angle was shown. In order to fully investigate the effect of the yaw angle, the variation of measured quantities with respect to azimuth angle is considered. In this case, the BIN average of experimental data was calculated for every 12 degrees of azimuth angle. It means that data averaged for a specific azimuth angle, Ψ, were obtained from BIN averaging of the data included in the interval $(\Psi-6, \Psi+6)$ degrees.

Figure 10 show the measured section characteristics against azimuth angle. Results for three representative yaw angles, Φ, of -45, 0, and 45 degrees, respectively, are compared. Figure 10(a) shows inflow velocity W against azimuth angle Ψ. The uniform inflow velocity is apparent for whole range of azimuth angle when yaw angle is $\Phi=0$ degree. The harmonic change of the inflow velocity for positive or negative yaw angles is also evident. In the situation of azimuth angle $\Psi=0$ degree at the yaw angle $\Phi=45$ degrees, since the wind acts as an against wind to the rotating blade, inflow speed W becomes large. On the other hand, in the situation of azimuth angle $\Psi=180$ degrees, since the wind acts as a following wind to the rotating blade, inflow speed W becomes small. On the contrary, in the situation of azimuth angle $\Psi=0$ degree at the yaw angle $\Phi=-45$ degrees, since a wind acts as a following wind to the rotating blade, inflow speed W becomes small, and vice versa, in the situation of azimuth angle $\Psi=180$ degrees, since the wind acts as an against wind to the rotating blade, inflow speed W becomes large. Figure 10(b) shows local angle of attack α against azimuth angle Ψ. In the yaw angle $\Phi=0$ degree, the value of α is large at the azimuth angle $\Psi=0$ degree and small at the azimuth angle $\Psi=180$ degrees. It is caused by the influence of atmospheric boundary layer. It means that wind speed is larger at the azimuth angle $\Psi=0$ degree,

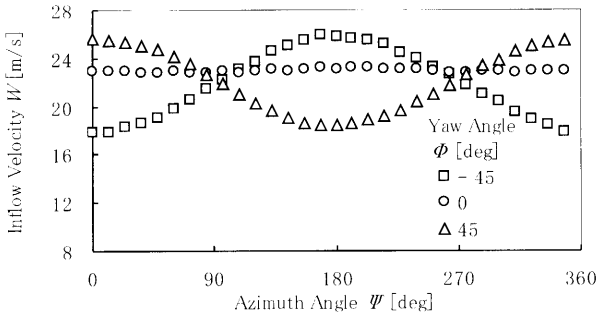

(a) Inflow velocity W

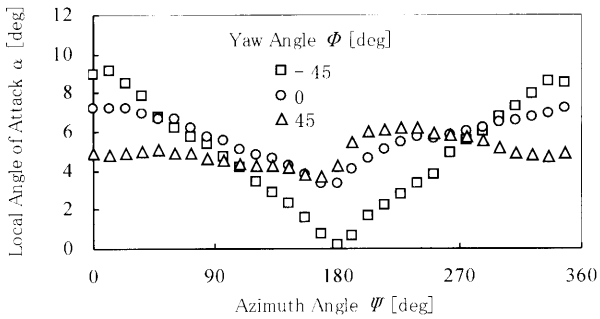

(b) Local angle of attack α

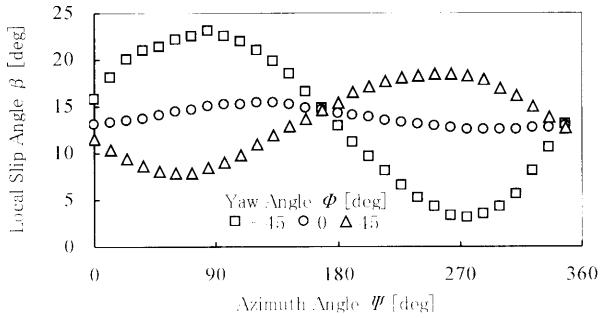

(c) Local slip angle β

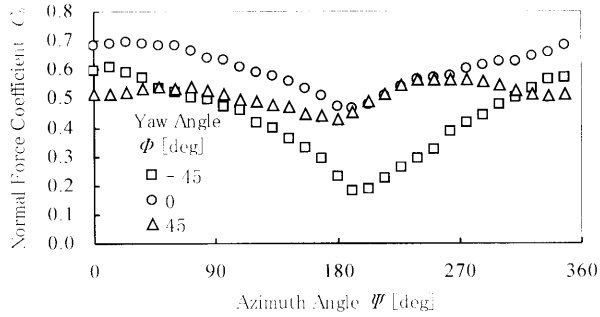

(d) Normal force coefficient C_n

Fig. 10 Change of section characteristics due to azimuth angle Ψ in several yawed conditions

which corresponds to the situation of blade top position, and smaller at the azimuth angle $\Psi=180$ degrees, which correspond to the situation of blade bottom position. In the yaw angle $\Phi=45$ degrees, the value of α is small at the azimuth angle $\Psi=180$ degrees and it reaches its peak near the azimuth angle $\Psi=200$ degrees. In this situation, inflow velocity W, as shown in Fig. 10(a), is close to the minimum value. As for the operational condition in the

yaw angle $\Phi = -45$ degree, it is noted that corresponding to the small values of inflow velocity at the azimuth angle 0 degrees (Fig. 10 (a)), local angle of attack α takes larger value, and it takes smaller value at azimuth angle 180 degrees where the inflow velocity W is larger. Figure 10 (c) shows local slip angle β against azimuth angle Ψ. In the yaw angle $\Phi = 0$ degree, the relation between yaw angle Φ and local slip angle β is substantially constant. In the yaw angle $\Phi = 45$ degrees, β value is close to minimum value at the azimuth angle $\Psi = 90$ degrees and maximum value at the azimuth angle $\Psi = 270$ degrees. Although inflow velocity W in these angles is the same, the blade tip at the azimuth angle $\Psi = 90$ degrees is in the upstream side as compared with the nacelle, since the position of the blade tip is in the same height with the hub. On the other hand, the blade tip at the azimuth angle $\Psi = 270$ degrees is in the downstream side as compared with the nacelle. In case of data obtained in the yaw angle $\Phi = -45$ degrees, local slip angle changes in opposite direction to that of the yaw angle $\Phi = 45$ degrees, and the rate of change is much larger. Figure 10 (d) shows normal force coefficient C_n against azimuth angle Ψ. From the result of Fig. 10 (a) and (b), the value of α and W are almost independent of yaw angle Φ, in the situation of azimuth angle Ψ of 90 and 270 degrees. Comparing the values of β and C_n (Fig. 10 (c) and (d)), large difference can be seen resulting from the difference in yaw angle Φ at the azimuth angle $\Psi = 270$ degrees. Moreover, from Fig. 10 (b) and (d), when the range of Ψ is $\Psi \leq 90$ degrees and $\Psi \geq 270$, it can be seen that though α value takes the largest value at the yaw angle $\Phi = -45$ degrees, C_n value takes the largest value at the yaw angle $\Phi = 0$ degree. It seems that although C_n value depends only on α in a two-dimensional flow, C_n value does not depend only on α for the rotating blade. This is the reason why C_n value significantly decreases in Fig. 8.

4.4 Change of the pressure distribution due to yaw angle

Figure 11 shows comparison of the pressure distribution due to yaw angle Φ, which corresponds to local angle of attack α of 10 degrees in Fig. 8. Comparing the pressure distributions obtained in cases of yaw angle Φ of 0 degree and 45 degrees, it is noted they are almost identical but is a little decrease of the suction pressure on the suction surface in the range of $0.3 < x/c < 0.6$ at the yaw angle $\Phi = 45$ degrees. Big difference is noticed when comparing pressure distributions in case of yaw angle Φ of 0 degree and -45 degrees. The chordwise pressure on the suction surface for yaw angle $\Phi = -45$ degrees is less than in case of yaw angle $\Phi = 0$ degrees. On the other hand, pressure on pressure surface increases in the range of $0.4 \leq x/c \leq 0.9$. Therefore, it can be seen that a clear difference appears in the pressure distribution between yaw angle $\Phi = 0$ and $\Phi = -45$ degrees.

Figure 12 shows the pressure distribution at the azimuth angle $\Psi = 270$ degrees, at which the values of W and α, as it was shown in Fig. 10, seemed to be independent of the all the yaw angles, however, but C_n values were differed for different yaw angles. The differences on the pressure distributions are apparent when comparing the data obtained in the yaw angle 0 and -45 degrees. The pressure on the suction surface decreases is less in case of yaw angle -45 degrees than in case of yaw angle 0 degrees. On the other hand, the pressure on the pressure surface increases in the range of $0.5 \leq x/c \leq 0.9$. Now comparing the data obtained in the yaw angle 0 and 45 degrees, it is noted that in case of yaw angle 45 degrees there is a decrease of the pressure on the suction surface at $0.3 \leq x/c \leq 0.5$ chordwise stations. Therefore, even when the values of α and W are mostly independent of the yaw angle, it can be seen that a clear difference appears in the pressure distribution.

4.5 Tufts flow-visualization on the rotating blade

Figure 13 shows a picture of the flow-visualization by

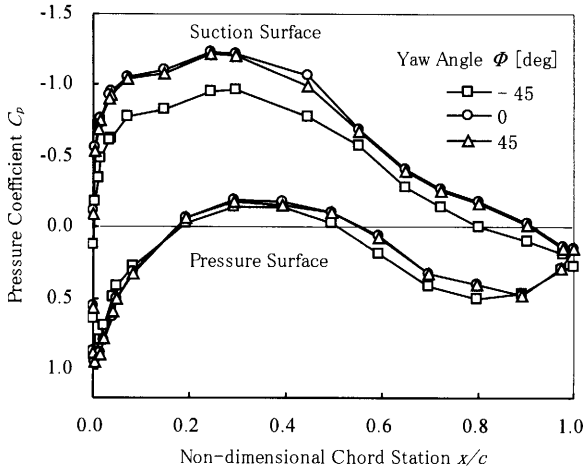

Fig. 11 Pressure distribution at $\alpha = 10$ degrees in several yawed conditions

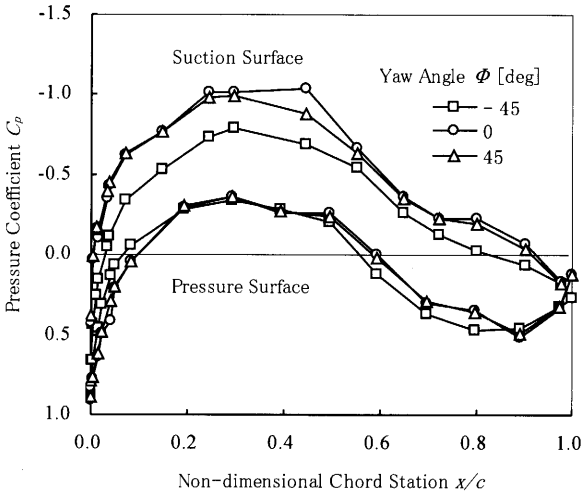

Fig. 12 Pressure distribution at $\alpha = 5.5$ degrees at $\psi = 270$ degrees in several yawed conditions

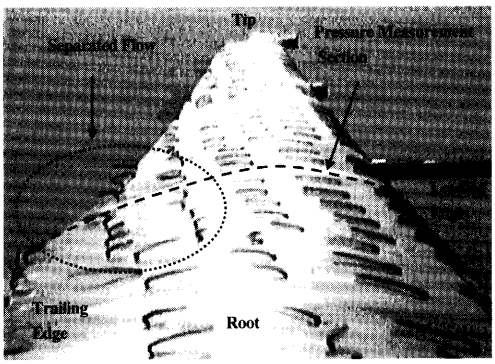

Fig. 13 Flow visualization on suction surface at $\Psi = 0$ degree ($\alpha = 10.6$ degrees, $\beta = 9.5$ degrees, $\Phi = -49.1$ degrees and $Re = 3.5 \times 10^5$)

surface tuft method, taken when the nacelle was directed at yaw angle $\Phi = -45$ degrees. The blade position corresponds to azimuth angle $\Psi = 0$ degree, with the blade tip in the uppermost vertical position. Even though the local angle of attack is as small as $\alpha = 10.6$ degrees, the separation has occurred in the region of the maximum camber to the trailing edge. This separation has been observed in the range of the azimuth angle between $0 \leq \Psi \leq 90$ degrees. No separation was observed when the azimuth angle was $90 < \Psi < 360$ degrees. In the range of azimuth angle $300 \leq \Psi \leq 360$ degrees, it was observed that tufts were floating from the blade surface without fluctuation. It is concluded that the main reason of the decreasing tendency of the C_n values in case of the yaw angle $\Phi = -45$ degrees, as shown in Figs. 8 and 10(d), is the observed separation at the trailing edge.

5. Conclusions

Local aerodynamic characteristics of a rotating blade were compared paying attention to the effect of the yaw angle. These comparisons were based on field test data acquired by measuring the pressure distribution at the 50% radial section on the rotating blade. Following results can be drawn from this study:

(1) In yawed condition it is proved that the normal force coefficients are smaller than in non-yawed condition.

(2) Based on the non-yawed condition, an asymmetry on the decreasing tendency of the C_n for every local angle of attack α is found. Rate of decrease in case of negative yaw angles is larger than in case of positive yaw angles. Negative yaw angles affect the turbine performance considerably.

(3) Even when, at specific azimuth angles, the local angle of attack α and inflow velocity W are almost the same and independent of the yaw angle Φ, there are significant differences on the pressure distributions and the local slip angle β.

(4) From the result of the tufts flow-visualization on the rotor blade, it became clear that the separation occurred in the range of azimuth angle of $0 \leq \Psi \leq 90$ at the yaw angle $\Phi = -45$ degrees and the value of C_n is decreased significantly.

Acknowledgement

The authors would like to thank Mr. A. Bruining and R. van Rooij of Delft University of Technology for their contribution on designing and setting up test turbine.

References

(1) Madsen, H.A. and Christensen, H., On the Relative Importance of Rotational, Unsteady and Three-Dimensional Effects on the HAWT Rotor Aerodynamics, Wind Engineering, Vol.14, No.6 (1990), pp.405–415.

(2) Huyer, S.A., Simms, D. and Robinson, M.C., Unsteady Aerodynamics Associated with a Horizontal-Axis Wind Turbine, AIAA Journal, Vol.34, No.7 (1996), pp.1410–1419.

(3) Schreck, S. and Robinson, M.C., Rotational Augmentation of Horizontal Axis Wind Turbine Blade Aerodynamic Response, Wind Energy, Vol.5 (2002), pp.133–150.

(4) Maeda, T., Kawabuchi, H., Shimizu, Y. and Bruining, A., Measurement of Pressure Distribution on Rotating Blade of Field Horizontal Axis Wind Turbine, Trans. Jpn. Soc. Mech. Eng., (in Japanese), Vol.70, No.693, B (2004), pp.119–125.